

# Gauge and matter fields as surfaces and loops - an exploratory lattice study of the $Z_3$ Gauge-Higgs model

Christof Gattringer, Alexander Schmidt

*Institut für Physik, FB Theoretische Physik, Universität Graz, 8010 Graz, Austria*

(Dated: September 1, 2012)

We discuss a representation of the  $Z_3$  Gauge-Higgs lattice field theory at finite density in terms of dual variables, i.e., loops of flux and surfaces. In the dual representation the complex action problem of the conventional formulation is resolved and Monte Carlo simulations at arbitrary chemical potential become possible. A suitable algorithm based on plaquette occupation numbers and link-fluxes is introduced and we analyze the model at zero temperature and finite density both in the weak and strong coupling phases. We show that at zero temperature the model has different first order phase transitions as a function of the chemical potential both for the weak- and strong coupling phases. The exploratory study demonstrates that alternative degrees of freedom may successfully be used for Monte Carlo simulations in several systems with gauge and matter fields.

PACS numbers: 11.15.Ha

## I. INTRODUCTORY REMARKS

In the last three decades lattice QCD has seen an impressive development into a reliable tool for obtaining non-perturbative results in hadron physics. However, for one important application, the study of QCD at finite density, the lattice formulation has so far not lived up to our expectations. The reason is that for non-zero chemical potential the fermion determinant is complex and cannot be interpreted as a probability in a Monte Carlo simulation. Various approaches to circumvent this problem were explored and the reviews at the annual lattice conferences provide a regular update [1, 2].

An interesting approach to lattice systems with a complex action problem is to search for a mapping to alternative variables where the partition sum is a sum over real and positive contributions such that in terms of the new variables the complex action problem is gone. Even for theories without a complex action problem an alternative representation of the partition sum could allow for improved Monte Carlo simulations with new algorithmic ideas. A prominent simple example is the worm algorithm [3] for spin systems such as the Ising model which is based on a representation of the partition sum in terms of closed loops of  $Z_2$  flux.

In recent years several examples for new algorithmic approaches that are based on transformations of lattice field theories to new variables were presented for a wide range of applications: Low dimensional systems [4], strongly coupled lattice field theories [5], systems with 4-fermi interactions [6], effective theories for QCD [7, 8], scalar field theories [9, 10] and U(1) lattice gauge theory [11, 12]. Similar in spirit, simulations directly based on the Trotter formula for lattice field theories in Hamiltonian approach were explored [13]. Many interesting conceptual and algorithmic ideas emerged in these papers and systems that previously were not fully accessible to Monte Carlo simulations can now be explored.

So far the studies with alternative variables (dual variables) were mostly concerned with flux-like structures living on links, with the exception of the studies [11, 12] of pure U(1) gauge theory where the dual variables are surfaces. In theories where gauge fields interact with matter fields, such as QCD, QED or Gauge-Higgs systems a dual representation will contain both: Surfaces for the gauge fields and fluxes for matter fields which serve as boundaries for open surfaces.

In this article we develop the idea of using dual representations for simulations of lattice field theories further and explore dual representations for the  $Z_3$  Gauge-Higgs systems. This is a first step towards systems which couple gauge- and matter fields and where surfaces interacting with fluxes appear in the dual representation. As a matter of fact all abelian Gauge-Higgs theories have a dual representation similar to the one we here discuss for the  $Z_3$  case and the techniques presented here can be adapted to other abelian cases. The choice to use the gauge group  $Z_3$  in this exploratory study is partly motivated by the possibility to couple a chemical potential and to explore finite density physics for  $Z_3$ , which as the center group of SU(3) plays an interesting role in the phenomenology of QCD. At zero temperature we explore the various phase transitions as a function of the chemical potential. The main goal of this work is to develop further alternative representations of lattice field theories and their use in Monte Carlo simulations.

In the next section we derive the dual representation of the partition sum in terms of fluxes and surfaces. In Section III we discuss observables and develop our strategy for the Monte Carlo simulation in terms of the dual variables. In Section IV we first compare the dual simulation of pure  $Z_3$  lattice gauge theory and the full system at  $\mu = 0$  to results from a Monte Carlo calculation in the conventional approach. This is followed by the presentation of the results at finite density (Section V). A summary in Section VI completes the paper.

## II. DUAL REPRESENTATION OF THE $Z_3$ GAUGE-HIGGS MODEL

In this section we discuss the derivation of the dual representation for the  $Z_3$  Gauge Higgs model on the lattice. Both the Higgs- and the gauge variables are elements of the group  $Z_3 = \{1, e^{i2\pi/3}, e^{-i\pi/3}\}$ , and it is possible to couple a chemical potential  $\mu$ . In the conventional representation the model then has a complex action problem at  $\mu > 0$ .

The Higgs field variables  $\phi_x$  live on the sites of a  $N_s^3 \times N_t$  lattice and are parameterized as  $\phi_x = e^{is_x 2\pi/3}$  with  $s_x \in \{-1, 0, +1\}$ . The gauge fields live on the links and are written as  $U_{x,\sigma} = e^{ia_{x,\sigma} 2\pi/3}$  with  $a_{x,\sigma} \in \{-1, 0, +1\}$ . For both fields periodic boundary conditions are used in all 4 directions. The action  $S = S_G + S_H$  is split into a gauge action  $S_G$  and the action for the Higgs field  $S_H$ . For the gauge action we use Wilson's form (without constant term),

$$S_G = -\frac{\beta}{2} \sum_x \sum_{\sigma < \tau} \left[ U_{x,\sigma\tau} + U_{x,\sigma\tau}^* \right], \quad (1)$$

where the double sum runs over all plaquettes  $U_{x,\sigma\tau} = U_{x,\sigma} U_{x+\hat{\sigma},\tau} U_{x+\hat{\sigma},\sigma}^* U_{x,\tau}^*$ . The action for the Higgs field in a gauge field background configuration is

$$S_H = -\eta \sum_{x,\nu} \left[ e^{\mu\delta_{\nu,4}} \phi_x^* U_{x,\nu} \phi_{x+\hat{\nu}} + e^{-\mu\delta_{\nu,4}} \phi_x^* U_{x-\hat{\nu},\nu}^* \phi_{x-\hat{\nu}} \right]. \quad (2)$$

The hopping terms in the 4-direction (= temporal direction) are coupled to the chemical potential  $\mu$ . The factor  $\eta$  controls the coupling between the Higgs- and the gauge fields. Essentially it plays the role of an inverse Higgs mass: If the Higgs field is infinitely heavy ( $\eta = 0$ ) it decouples from the dynamics of the system. The partition sum is obtained by summing the Boltzmann factor over all possible configurations

$$Z = \sum_{\{s,a\}} e^{-S_G - S_H}, \quad (3)$$

with

$$\sum_{\{s,a\}} = \left( \prod_x \sum_{s_x=-1}^1 \right) \left( \prod_{x,\sigma} \sum_{a_{x,\sigma}=-1}^1 \right). \quad (4)$$

For deriving the dual representation of the Higgs field action we use two identities which may be checked by explicit evaluation of both sides of the equations for the three cases  $s = -1, 0, 1$ . For the spatial nearest neighbor terms without chemical potential we use ( $s = -1, 0, 1$ )

$$\exp\left(\eta e^{i\frac{2\pi}{3}s} + \eta e^{-i\frac{2\pi}{3}s}\right) = C_\eta \sum_{k=-1}^1 B_\eta^{|k|} e^{i\frac{2\pi}{3}sk},$$

$$C_\eta = \frac{e^{2\eta} + 2e^{-\eta}}{3}, \quad B_\eta = \frac{e^{2\eta} - e^{-\eta}}{e^{2\eta} + 2e^{-\eta}}. \quad (5)$$

For the temporal hops where the chemical potential enters we need ( $s = -1, 0, 1$ )

$$\exp\left(\eta e^\mu e^{i\frac{2\pi}{3}s} + \eta e^{-\mu} e^{-i\frac{2\pi}{3}s}\right) = \sum_{k=-1}^1 M_k e^{i\frac{2\pi}{3}sk},$$

$$M_k = \frac{1}{3} \left[ e^{2\eta \cosh(\mu)} + 2e^{-\eta \cosh(\mu)} \cos\left(\sqrt{3}\eta \sinh(\mu) - k\frac{2\pi}{3}\right) \right]. \quad (6)$$

These auxiliary formulas are now used in an expansion of the Boltzmann factor. We find (the index  $j$  runs from 1 to 3,  $V = N_s^3$  is the spatial volume and we use the representations  $\phi_x = e^{is_x 2\pi/3}$  and  $U_{x,\nu} = e^{ia_{x,\nu} 2\pi/3}$ )

$$\prod_{x,\nu} \exp\left(\eta e^{\mu\delta_{\nu,4}} e^{i\frac{2\pi}{3}[s_{x+\hat{\nu}} - s_x + a_{x,\nu}]}\right. \\ \left. + \eta e^{-\mu\delta_{\nu,4}} e^{-i\frac{2\pi}{3}[s_{x+\hat{\nu}} - s_x + a_{x,\nu}]}\right) \\ = C_\eta^{3V} \sum_{\{k\}} \left( \prod_{x,j} B_\eta^{|k_{x,j}|} e^{i\frac{2\pi}{3}[s_{x+\hat{j}} - s_x + a_{x,j}]k_{x,j}} \right) \\ \times \left( \prod_x M_{k_{x,4}} e^{i\frac{2\pi}{3}[s_{x+\hat{4}} - s_x + a_{x,4}]k_{x,4}} \right). \quad (7)$$

We have introduced the shorthand notation  $\sum_{\{k\}} = \prod_{x,\nu} \sum_{k_{x,\nu}=-1}^1$  for the sum over all configurations of the expansion indices  $k$ . Inserting the expanded Boltzmann factor into the partition sum for the Higgs field in a given gauge field background (represented by the coefficients  $a_{\nu,x}$ ) we find

$$Z_H[a] = \sum_{\{s\}} e^{-S_H} = C_\eta^{3V} \sum_{\{k\}} \left( \prod_{x,j} B_\eta^{|k_{x,j}|} \right) \left( \prod_x M_{k_{x,4}} \right) \\ \times \left( \prod_{x,\nu} e^{i\frac{2\pi}{3}a_{x,\nu}k_{x,\nu}} \right) \left( \prod_x \sum_{s_x=-1}^1 e^{-i\frac{2\pi}{3}s_x \sum_\nu [k_{x,\nu} - k_{x-\hat{\nu},\nu}]} \right), \quad (8)$$

where we have suitably reorganized the product over the link terms. The product of sums in the last term of this expression is the remaining sum over the configurations of the Higgs fields (parameterized by  $s_x$ ). Each of the individual sums over the  $s_x$  vanishes, unless  $\sum_\nu [k_{x,\nu} - k_{x-\hat{\nu},\nu}]$  is a multiple of 3. It is useful to define the triality function  $T(n)$  as

$$T(n) = \begin{cases} 1 & \text{if } n \bmod 3 = 0, \\ 0 & \text{if } n \bmod 3 \neq 0. \end{cases} \quad (9)$$

Using the triality function  $T(n)$  we write the Higgs-field

partition sum as

$$Z_H[a] = C_\eta^{3V} 3^V \sum_{\{k\}} \left( \prod_{x,j} B_\eta^{|k_{x,j}|} \right) \left( \prod_x M_{k_{x,4}} \right) \times \left( \prod_{x,\nu} e^{i \frac{2\pi}{3} a_{x,\nu} k_{x,\nu}} \right) \left( \prod_x T \left( \sum_\nu [k_{x,\nu} - k_{x-\hat{\nu},\nu}] \right) \right). \quad (10)$$

The last factor implements a constraint at each site  $x$ , i.e., the net-flux through  $x$ , given by  $\sum_\nu [k_{x,\nu} - k_{x-\hat{\nu},\nu}]$ , has to vanish modulo 3.

If the net flux through a site were to vanish exactly (not only modulo 3) the constraint would imply that only closed loops of flux are allowed. The fact that the net flux through each site vanishes only modulo 3 augments the closed loop condition with an additional rule allowing 3 units of flux to emerge from a site or to vanish at a site.

The next step is to use the flux representation (10) for the Higgs part in the expression for the full partition sum. The Boltzmann factor for the gauge part is also expanded, re-using the identity (5) in the form ( $a = -1, 0, 1$ )

$$\exp \left( \frac{\beta}{2} e^{i \frac{2\pi}{3} a} + \frac{\beta}{2} e^{-i \frac{2\pi}{3} a} \right) = C_\beta \sum_{p=-1}^1 B_\beta^{|p|} e^{i \frac{2\pi}{3} a p}, \quad (11)$$

$$C_\beta = \frac{e^\beta + 2e^{-\frac{\beta}{2}}}{3}, \quad B_\beta = \frac{e^\beta - e^{-\frac{\beta}{2}}}{e^\beta + 2e^{-\frac{\beta}{2}}}.$$

Representing the Boltzmann factor for the gauge fields with this formula and inserting it in the full partition sum we find after some reordering of terms

$$Z = \sum_{\{a\}} e^{-S_G} Z_H[a] = C_\eta^{3V} 3^V C_\beta^{6V} \sum_{\{p,k\}} \left( \prod_{x,j} B_\eta^{|k_{x,j}|} \right) \times \left( \prod_x M_{k_{x,4}} \right) \left( \prod_{x,\sigma < \tau} B_\beta^{|p_{x,\sigma\tau}|} \right) \left( \prod_x T \left( \sum_\nu [k_{x,\nu} - k_{x-\hat{\nu},\nu}] \right) \right) \times \left( \prod_{x,\nu} \sum_{a_{x,\nu}=-1}^1 \exp \left( i \frac{2\pi}{3} a_{x,\nu} \times \left[ \sum_{\nu < \alpha} [p_{x,\nu\alpha} - p_{x-\hat{\alpha},\nu\alpha}] - \sum_{\alpha < \nu} [p_{x,\alpha\nu} - p_{x-\hat{\alpha},\alpha\nu}] + k_{x,\nu} \right] \right) \right).$$

We have introduced plaquette occupation numbers  $p_{x,\sigma\tau}$  which may assume the values  $-1, 0$  and  $+1$  and for unique labeling of the plaquettes we only consider  $p_{x,\sigma\tau}$  with  $\sigma < \tau$ . As before, by  $\sum_{\{p\}}$  we denote the sum over all configurations of the  $p_{x,\sigma\tau}$ . The last product of sums in (12) gives rise to triality constraints for all links which combine the plaquette occupation numbers of all plaquettes attached to that link and the  $k$ -flux residing on that link. In a more compact notation the final result for the partition sum of the  $Z_3$  Gauge-Higgs model reads

$$Z = C \sum_{\{p\}} \sum_{\{k\}} \mathcal{C}_P[p, k] \mathcal{C}_F[k] \mathcal{W}_P[p] \mathcal{W}_F[k]. \quad (13)$$

The first sum runs over all configurations of the integer valued plaquette occupation variables  $p_{x,\sigma\tau} \in \{-1, 0, +1\}$  assigned to the plaquettes of the lattice, while the second sum is over all configurations of the flux variables  $k_{x,\nu} \in \{-1, 0, +1\}$  living on the links of the lattice. The flux variables  $k$  are subject to the constraint  $\mathcal{C}_F[k]$  given by

$$\mathcal{C}_F[k] = \prod_x T \left( \sum_\nu [k_{x,\nu} - k_{x-\hat{\nu},\nu}] \right), \quad (14)$$

which enforces the conservation of  $k$ -flux modulo 3 at each site of the lattice (see (9) for the definition of  $T(n)$ ). This flux conservation restricts the admissible configurations to closed oriented loops of  $k$ -flux. A second constraint,

$$\mathcal{C}_P[p, k] = \prod_{x,\nu} T \left( \sum_{\nu < \alpha} [p_{x,\nu\alpha} - p_{x-\hat{\alpha},\nu\alpha}] - \sum_{\alpha < \nu} [p_{x,\alpha\nu} - p_{x-\hat{\alpha},\alpha\nu}] + k_{x,\nu} \right), \quad (15)$$

connects the plaquette occupation numbers  $p$  with the  $k$ -variables: At every link it enforces the combined flux of the plaquette occupation numbers attached to that link plus the  $k$ -flux on that link to vanish modulo 3. Similar to the closed loop interpretation for the  $k$ -flux, the link constraint forces the plaquette occupation numbers  $p$  into forming closed surfaces, or open surfaces bounded by loops of  $k$ -flux, and again the surface rule is augmented by the modulo 3 exemption as for the fluxes.

Both, the plaquette occupation numbers and the fluxes come with corresponding weight factors, given by

$$\mathcal{W}_P[p] = \prod_{x,\sigma < \tau} B_\beta^{|p_{x,\sigma\tau}|}, \quad (16)$$

$$\mathcal{W}_F[k] = \left( \prod_{x,j} B_\eta^{|k_{x,j}|} \right) \left( \prod_x M_{k_{x,4}} \right),$$

where the explicit expressions for  $B_\eta$  and  $B_\beta$  are given in (5) and (11). The partition sum (13) comes with an overall normalization factor  $C = (3^5 C_\eta^3 C_\beta^6)^V$  where  $V = N_s^3$  and  $C_\eta$  and  $C_\beta$  are given in (5) and (11).

### III. OBSERVABLES AND MONTE CARLO UPDATE

Having mapped the partition sums onto the dual variables we now also need to identify the representation of the observables in terms of the dual degrees of freedom. In this exploratory study we concentrate on thermodynamical observables, i.e., observables that are obtained as derivatives of  $\ln Z$  with respect to the various couplings [20]. For the gauge sector we obtain the average plaquette  $\langle U \rangle$  and the corresponding susceptibility  $\chi_U$  as first

and second derivatives with respect to the inverse gauge coupling  $\beta$ ,

$$\langle U \rangle = \frac{1}{6N_s^3 N_t} \frac{\partial}{\partial \beta} \ln Z, \quad \chi_U = \frac{1}{6N_s^3 N_t} \frac{\partial^2}{\partial \beta^2} \ln Z. \quad (17)$$

Both observables are normalized by the total number of plaquettes. The  $\beta$ -dependence of the dual representation is encoded in the weight factors given by the product (16) over powers  $B_\beta^{|p|}$  of the factors  $B_\beta$  defined in (11). There is an additional  $\beta$ -dependence from the overall factor  $C$  which also contains  $B_\beta$ . This factor is necessary for the correct representation of the observables listed in (17).

It is straightforward to evaluate the expressions (17) in the dual representation and one obtains:

$$\begin{aligned} \langle U \rangle &= B_\beta + \frac{1}{6N_s^3 N_t} \frac{B'_\beta}{B_\beta} \left\langle \sum_{x, \sigma < \tau} |p_{x, \sigma \tau}| \right\rangle, \quad (18) \\ \chi_U &= B'_\beta + \frac{1}{6N_s^3 N_t} \frac{B''_\beta B_\beta - (B'_\beta)^2}{B_\beta^2} \left\langle \sum_{x, \sigma < \tau} |p_{x, \sigma \tau}| \right\rangle + \\ &\frac{1}{6N_s^3 N_t} \left( \frac{B'_\beta}{B_\beta} \right)^2 \left[ \left\langle \left( \sum_{x, \sigma < \tau} |p_{x, \sigma \tau}| \right)^2 \right\rangle - \left\langle \sum_{x, \sigma < \tau} |p_{x, \sigma \tau}| \right\rangle^2 \right]. \end{aligned}$$

For the Higgs sector we study the particle number density  $n$  and the corresponding susceptibility  $\chi_n$  which may be obtained as derivatives with respect to  $\mu$  (again normalized with the 4-volume):

$$n = \frac{1}{N_s^3 N_t} \frac{\partial}{\partial \mu} \ln Z, \quad \chi_n = \frac{1}{N_s^3 N_t} \frac{\partial^2}{\partial \mu^2} \ln Z. \quad (19)$$

The corresponding observables in the dual representation are

$$\begin{aligned} n &= \frac{1}{N_s^3 N_t} \langle R_1 \mathcal{N}_1 + R_0 \mathcal{N}_0 + R_{-1} \mathcal{N}_{-1} \rangle, \quad (20) \\ \chi_n &= \frac{1}{N_s^3 N_t} \left[ \langle Q_1 \mathcal{N}_1 + Q_0 \mathcal{N}_0 + Q_{-1} \mathcal{N}_{-1} \rangle \right. \\ &\quad + \langle (R_1 \mathcal{N}_1 + R_0 \mathcal{N}_0 + R_{-1} \mathcal{N}_{-1})^2 \rangle \\ &\quad \left. - \langle R_1 \mathcal{N}_1 + R_0 \mathcal{N}_0 + R_{-1} \mathcal{N}_{-1} \rangle^2 \right]. \end{aligned}$$

We introduced the abbreviations  $\mathcal{N}_s$ ,  $s = -1, 0, 1$  for the total number of temporal link variables  $k_{x,4}$  that have a value  $s = -1, 0, 1$ . The  $R_k$  and  $Q_k$  with  $k = -1, 0, 1$  denote the ratios  $R_k = M'_k/M_k$  and  $Q_k = [M''_k M_k - (M'_k)^2]/M_k^2$ , where the  $M_k$  are the factors defined in (6) and the primes are used for their derivatives with respect to  $\mu$ .

Although the partition sums and the observables may seem somewhat involved in the dual representation, the dual Monte Carlo update turns out to be rather simple. We begin its discussion with introducing an update for pure gauge theory which in the next section we study as

a first test case. The pure gauge update then serves as the starting point for developing the full algorithm where we will augment the pure gauge algorithm with another simple step to update the Higgs field as well.

In the dual representation the pure gauge theory is a theory of only the plaquette variables and the partition sum can be written as (see (13)),

$$Z_G = \sum_{\{p\}} C_P[p] W_P[p], \quad (21)$$

where the sum is over configurations of the plaquette occupation numbers  $p_{x, \sigma \tau} \in \{-1, 0, 1\}$ . The constraint  $C_P[p]$  is simply the plaquette constraint (15) evaluated for the case when all  $k$ -fluxes are set to  $k_{x, \nu} = 0$ . The constraint is a product over all links and for each link the oriented flux of all plaquettes attached to that link has to be a multiple of 3 (see (15)). As discussed in the previous section the constraints give rise to the occupied plaquettes forming surfaces. Here, where we consider pure gauge theory, we have only closed surfaces since without matter fields there are no  $k$ -fluxes that could serve as boundaries of open surfaces.

For the update of the plaquette variables we start from a configuration of the plaquette occupation numbers  $p_{x, \sigma \tau}$  where all the link constraints are satisfied, using the simplest choice, i.e., the trivial configuration with  $p_{x, \sigma \tau} = 0$  for all  $x$  and all  $\sigma, \tau$ . Starting from the trivial configuration we offer trial configurations which leave the constraints intact and accept them with the usual Metropolis probability.

The trial configurations are generated by increasing or decreasing the plaquette occupation numbers on the faces of 3-cubes which we embed in four dimensions. Let  $1 \leq \nu_1 < \nu_2 < \nu_3 \leq 4$  denote the three directions that define the 3-cube. Then there are four possible choices of the  $\nu_i$ , i.e., four different 3-cubes can be embedded in four dimensions. Once the three directions  $\nu_i$  are fixed we select a site  $x$  for the lower left front corner of the cube and change the plaquette occupation numbers on the faces of the cube by  $\pm 1$  according to one of the two possibilities depicted in Fig. 1.

To take into account the fact that the plaquette occupation numbers are restricted to  $-1, 0$  and  $+1$ , the addition of  $\pm 1$  is understood only modulo 3. Addition modulo 3 is defined as the usual addition of the numbers  $+1, 0$  and  $-1$ , except for the two cases  $+1 + 1 \equiv -1$  and  $-1 - 1 \equiv +1$ . It is easy to check that the two changes illustrated in Fig. 1 leave the constraints at the sides of the cubes intact. The two possible changes are proposed with equal probability and are then accepted with the usual Metropolis probability. The corresponding acceptance rate is a product of factors  $(B_\beta)^{\pm 1}$  according to the plaquette occupation numbers at the faces of the cubes (see Eq. 16). A full cube sweep is a loop over all four possible embeddings of 3-cubes and over the  $N_s^3 \times N_t$  possibilities to place a particular cube.

On a finite lattice with periodic boundary conditions there are additional admissible configurations of the

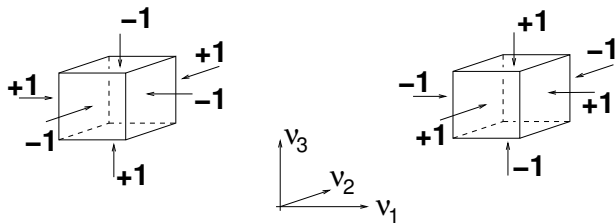


FIG. 1: Cube update: We illustrate the changes we propose for the plaquette occupation numbers at the faces of an embedded 3-cube with edges along the directions  $1 \leq \nu_1 < \nu_2 < \nu_3 \leq 4$ . The two choices in the lhs. and rhs. figure are proposed with equal probability.

plaquette occupation numbers which are not properly treated by the cube updates alone. They consist of surfaces that close around the periodic boundaries. To take them into account we offer an additional set of trial configurations, where we change all plaquette occupation numbers in a plane by  $\pm 1$  (addition is again understood modulo 3) and accept this change with the corresponding Metropolis probability which is a product of powers of  $B_\beta$  according to the plaquette occupation numbers on the plane of the trial configuration. For a complete "plane sweep" we offer this change for all possible planes (6 possible orientations of the planes with  $N_s^2$  or  $N_s N_t$  slices for each orientation). For the update of pure gauge theory we mix plane and cube sweeps.

For updating the full Gauge-Higgs systems also the matter fields need to be taken into account. They are represented by the link variables. The update of the  $k$ -fluxes is more interesting since they enter in two constraints: At each site the total flux of the  $k$ -variables has to vanish modulo 3. Furthermore, at each link the corresponding  $k$ -flux enters the constraint for the plaquette occupation numbers attached to that link. To deal with this situation we use proposal configurations that change a plaquette occupation number and the  $k$ -fluxes at the links of that plaquette. The two choices for such a change are depicted in Fig. 2, where  $1 \leq \nu_1 < \nu_2 \leq 4$  are the two directions that define the plane of the plaquette.

It is easy to see that the two moves we propose do not change the constraints on the sites or on the links (addition is again only understood modulo 3 as for the cube and plane updates). The two changes in Fig. 2 are proposed with equal probability and are accepted with the Metropolis acceptance rate. This is a product of a ratio of the plaquette weights  $B_\beta$  and a product over ratios of the 4 link weights, i.e., powers of  $B_\eta$  for the spatial links, and factors  $M_k$  for the temporal links. A full plaquette sweep then consists of a loop over all 6 embeddings of the planes of the plaquettes and all  $N_s^3 \times N_t$  possibilities to place the plaquette.

To summarize: For updating the full Gauge-Higgs model we use combined sweeps that mix full cube sweeps, full plane sweeps and full plaquette sweeps for the  $k$ -variables.

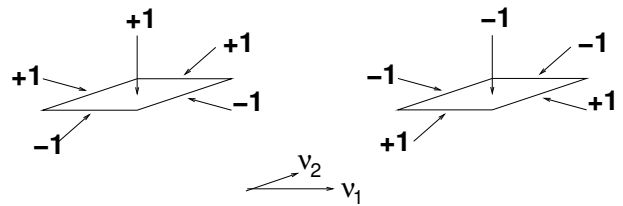


FIG. 2: Plaquette update: We illustrate the changes we propose for the plaquette occupation numbers at the plaquette and the corresponding changes of the flux variables at the links of the plaquette. The directions  $1 \leq \nu_1 < \nu_2 \leq 4$  determine the plane of the plaquette and the two choices in the lhs. and rhs. figure are proposed with equal probability.

It is interesting to note that when the Higgs field is coupled, i.e., for  $\eta > 0$ , the cube and plane sweeps could be omitted and it would be sufficient to work with the plaquette sweeps alone. The reason is that a cube update can be achieved by 6 plaquette updates, and a plane sweep by a combination of plaquette updates in the respective plane. However, we found that in particular omitting the cube updates may lead to a poorer performance of the algorithm in cases where the weights for the  $k$ -fluxes are small. We remark, that for the Higgs model without gauge fields a very efficient worm algorithm [3] can be constructed, and also for the full  $Z_3$ -case a surface type of generalization of the worm idea is possible [17] (see also [12] for tests in this direction).

#### IV. COMPARISON WITH CONVENTIONAL $\mu = 0$ RESULTS

##### A. Pure gauge theory

Having discussed the dual representation and the Monte Carlo algorithm in the dual picture we now come to the evaluation of the dual Monte Carlo approach. As a warm up exercise we begin with the case of pure gauge theory, where the Monte Carlo update is based on the cube and plane updates. The observables we consider are the plaquette expectation value  $\langle U \rangle$  and the corresponding susceptibility  $\chi_U$ . Their definitions and the corresponding dual expressions are given in (17) and (18).

In Fig. 3 we show the results for  $\langle U \rangle$  and  $\chi_U$  in pure  $Z_3$  lattice gauge theory ( $\eta = 0$ ), and compare the outcome of the dual simulation (circles) to the results from the conventional approach (crosses) using lattices with volumes of size  $10^4$ . The statistics is 10000 configurations separated by 10 cube sweeps and one plane sweep and another 10000 cube sweeps mixed with 1000 plane sweeps were used for equilibration. All errors we show in this work are statistical errors determined with the jackknife method.

Fig. 3 shows that the results of the dual simulation perfectly agree with the outcome of the conventional approach. Near  $\beta_c \sim 0.7$  the system apparently undergoes a

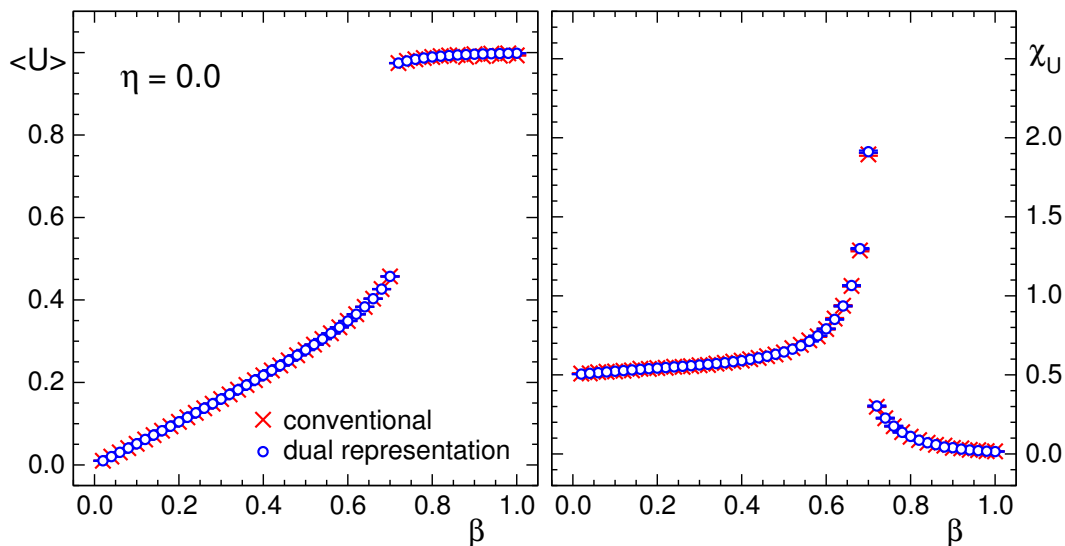


FIG. 3: Results for plaquette  $\langle U \rangle$  (lhs. plot) and the plaquette susceptibility  $\chi_U$  in pure  $Z_3$  gauge theory as a function of the inverse gauge coupling  $\beta$ . We compare the conventional (crosses) and the dual approach (circles).

quite prominent first order transition which separates the strong- ( $\beta < \beta_c$ ) and weak-coupling ( $\beta > \beta_c$ ) phases, and also near the transition the results for the first and second derivatives of the free energy (i.e.,  $\langle U \rangle$  and  $\chi_U$ ) obtained with the conventional and dual approaches agree perfectly. We conclude that for the case of pure  $Z_3$  lattice gauge theory the mapping to the dual representation, the identification of the observables and the simulation with the cube and plane algorithms work.

It is interesting to inspect the acceptance rate for the plane sweeps. We find that the acceptance is zero for the strong coupling phase, i.e., for  $\beta < \beta_c$ . For a small volume of size  $4^4$  we then see the onset of nonzero acceptance at  $\beta_c \sim 0.7$  reaching a value of 0.28 at  $\beta = 1.0$ . Repeating the same analysis on volumes of size  $10^4$  we again find non-zero acceptance only above  $\beta_c \sim 0.7$ , but the increase with  $\beta$  is much slower, and at  $\beta = 1.0$  we still see an acceptance rate smaller than 0.01. We conclude that the non-trivially winding sheets of occupation are a finite size effect that very quickly dies out with increasing volume.

At this point we remark, that the case of pure  $U(1)$  gauge theory in a dual representation which is similar to our  $Z_3$  form [21] has been studied numerically in [11, 12] (see also the discussion in [2]). The algorithms in [11] are very similar to our updates (however, partly without the global plane updates). In [12] defects (i.e., boundaries) are introduced for the surfaces and a generalization of the worm algorithm [3] to surfaces is explored.

### B. The full $Z_3$ Gauge-Higgs model at $\mu = 0$

Let us now come to the full  $Z_3$  Gauge-Higgs model. Again we would like to test the dual approach and verify

its validity by comparison with a conventional simulation, which is possible for  $\mu = 0$ .

For checking the correct implementation of the dual approach we compare the results for simulations at  $\mu = 0$  using two different values of the coupling  $\eta$ :  $\eta = 0.1$  and  $\eta = 0.5$  and plot the observables as a function of  $\beta$ . In Fig. 4 and Fig. 5 we show the results for  $\langle U \rangle$  (lhs. plots) and  $\chi_U$  (rhs.) as a function of  $\beta$ . Fig. 4 is for  $\eta = 0.1$  and Fig. 5 for  $\eta = 0.5$  and we compare the results from a conventional simulation (crosses) to the outcome from the dual approach (circles) and again use volumes of size  $10^4$  and the same sequence and amount of the different update sweeps as for pure gauge theory.

For  $\eta = 0.1$  the first order transition persists and we see very little change in our observables  $\langle U \rangle$  and  $\chi_U$  when comparing the results to pure gauge theory. Again we observe that the results from the dual simulation and the conventional approach match very well. However, since at  $\eta = 0.1$  and vanishing chemical potential  $\mu$  the influence of the Higgs field seems to be small, we consider a second, larger value of  $\eta$ .

The results for  $\langle U \rangle$  and  $\chi_U$  at  $\eta = 0.5$  and  $\mu = 0.0$  are shown in Fig. 5. We now observe quite a change in the behavior of the observables in comparison to the pure gauge and  $\eta = 0.1$  cases. The phase transition has apparently disappeared and we only find a smooth crossover-type of behavior between the strong- and weak coupling phases. The maximum of the susceptibility  $\chi_U$  has shifted to rather small values – the crossover takes place near  $\beta = 0.28$ . The important fact is, that also here at a larger value of  $\eta$ , where obviously the Higgs field has a much stronger influence, the results from the conventional approach and the dual simulation agree very well, again confirming the correctness of the implementation of the dual approach.

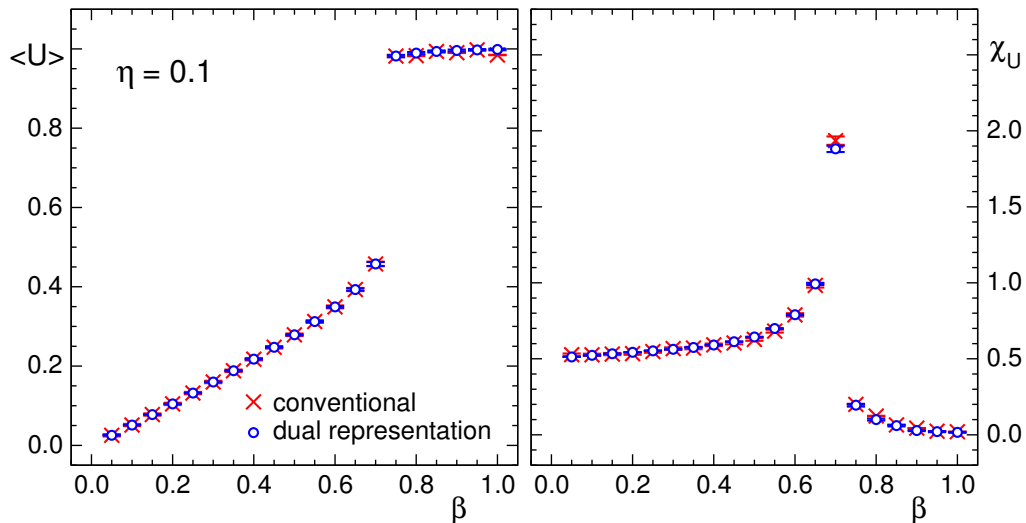


FIG. 4: Results for  $\langle U \rangle$  (lhs. plot) and  $\chi_U$  in full  $Z_3$  Gauge-Higgs theory at  $\eta = 0.1$  and  $\mu = 0.0$  as a function of the inverse gauge coupling  $\beta$ . We compare the conventional (crosses) and the dual approach (circles).

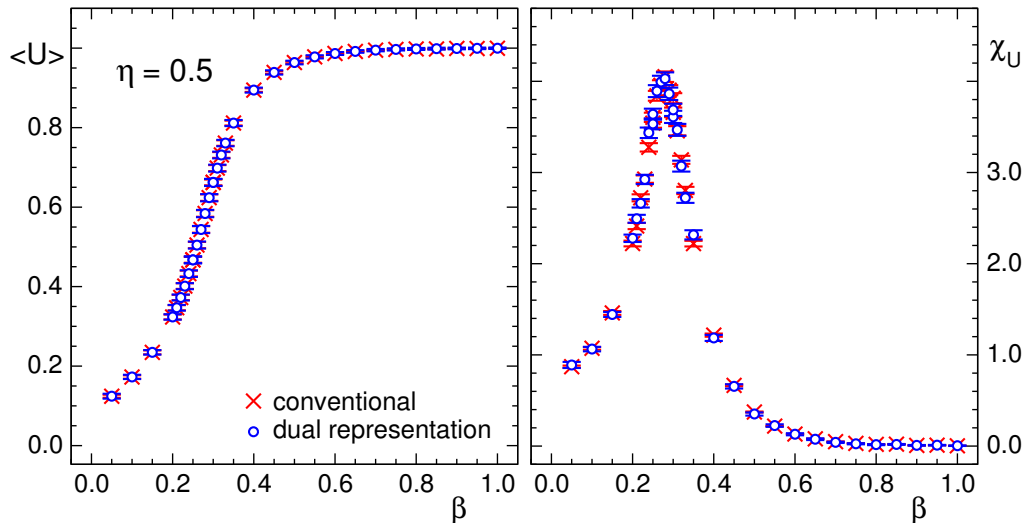


FIG. 5: Same as in Fig.4, but now for  $\eta = 0.5$ .

## V. THE $Z_3$ GAUGE-HIGGS MODEL AT FINITE DENSITY

Let us now come to the more interesting case of finite density. Here conventional simulations fail and the full potential of the dual approach can be unveiled. Before we start with the presentation of Monte Carlo results we first discuss some characteristic features of the dual representation at finite density.

### A. Finite density dynamics in the dual representation

The dual representation of the  $Z_3$  Gauge-Higgs model uses two sets of degrees of freedom, the plaquette occu-

pation numbers  $p$  and the fluxes  $k$ . For the analysis of the mechanisms that drive the systems at finite density it is useful to think a little bit about the dynamics of the dual variables, and this subsection is devoted to that task.

The dual degrees of freedom assume values in  $\{-1, 0, +1\}$ , i.e.,  $p_{x,\sigma\tau} \in \{-1, 0, +1\}$  and  $k_{x,\nu} \in \{-1, 0, +1\}$ . A trivial value of the plaquette occupation number, i.e.,  $p_{x,\sigma\tau} = 0$  comes with a Boltzmann factor of 1 (compare (16)), while non-trivial values  $p_{x,\sigma\tau} \pm 1$  give rise to a factor of  $B_\beta < 1$  (see (11) for the definition of  $B_\beta$ ). Thus non-trivial values of plaquette occupation numbers  $p$  are suppressed by their Boltzmann factor. On the other hand configurations with many  $p_{x,\sigma\tau} \neq 0$  have a much higher entropy and (as always) the interplay of entropy and Boltzmann factor gives rise to the first order

transition of the pure gauge theory discussed in Subsection IV-A. The corresponding observables  $\langle U \rangle$  and  $\chi_U$  are simple functions of the plaquette occupation numbers and their fluctuations. We stress at this point that both observables have a  $\beta$ -dependent additive term (compare (18)). For the plaquette expectation value the additive term is given by  $B_\beta$ , and  $\langle U \rangle$  is non-vanishing for  $\beta > 0$  even when all plaquette occupation numbers  $p$  are trivial, since  $B_\beta > 0$  for  $\beta > 0$ .

Similar to the plaquette occupation numbers, the spatial flux variables  $k_{x,j}$ ,  $j = 1, 2, 3$ , have a Boltzmann factor of 1 for  $k_{x,j} = 0$  and a Boltzmann factor  $B_\eta < 1$  for  $k_{x,j} = \pm 1$  (see (16)). As for the case of the plaquette occupation numbers, we find for the  $k$ -variables that trivial values of the spatial fluxes are preferred by the Boltzmann factor. The temporal flux variables  $k_{x,4}$  are connected with the Boltzmann factors  $M_s$  with  $s \in \{-1, 0, 1\}$  defined in (6). For  $\mu > 0$  we have  $M_{+1} > M_{-1}$  (see also the discussion below) and temporal flux with  $k_{x,4} = +1$  is favored over negative temporal flux, i.e.,  $k_{x,4} = -1$ .

To illustrate the physical picture in terms of the dual representation, in Fig. 6 we show a few low-lying excitations of the  $Z_3$  Gauge-Higgs model in the dual representation. Thick red lines oriented with arrows are used for the  $k$ -flux and filled blue squares for non-vanishing plaquette occupation numbers, and the circles in the squares indicate the orientation of the plaquette according to the sign of the corresponding plaquette occupation number  $p_{x,\sigma\tau}$ . The simplest excitations (the lhs. diagram in Fig. 6) are an occupied plaquette surrounded by flux. At each link the flux is compensated by the plaquette. Occupied plaquettes with suitable relative orientation can be attached to each other (see the example in the center diagram). At the link where they are joined the flux is absent and the contributions from the plaquette occupation numbers compensate. Finally the excitation in the rhs. diagram makes use of the fact that flux and plaquette numbers need to vanish only modulo 3. Three units of flux emerge from a site, travel in time and then terminate at another

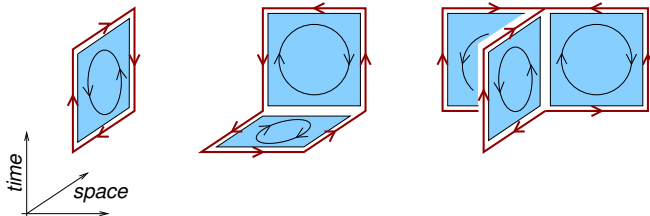


FIG. 6: Examples of low-lying excitations in the dual representation of the  $Z_3$  Gauge-Higgs model. We use red thick lines with arrows for the  $k$  flux variables and blue squares (with a circle showing the orientation) for the plaquette occupation numbers  $p$ . The rules for admissible configurations dictate that at each site the total flux from the  $k$ -variables has to be a multiple of 3. In addition for each link the combined flux of  $k$ -variables and plaquette occupation numbers  $p$  also has to be a multiple of 3.

site. The constraints are again saturated with plaquettes, such that at the central temporal link three plaquettes together obey the constraint. This excitation, which resembles a baryon, carries three factors of  $M_{+1}$  and thus is enhanced by the chemical potential.

Without chemical potential the Boltzmann factor for the excitations shown in Fig. 6 follows a simple rule: The more non-vanishing plaquette occupation numbers  $p$  and fluxes  $k$  a configuration has, the lower is the corresponding Boltzmann weight, and the dynamics discussed in Subsection IV-B. for the full  $Z_3$  Gauge Higgs system at  $\mu = 0$  is again determined by the interplay of entropy and Boltzmann weight.

The situation is more complex when the chemical potential  $\mu$  is turned on. Then the weights for the temporal flux variables  $k_{x,4}$  obey  $M_{+1} > M_{-1}$  and the probability for positive temporal fluxes is increased relative to the probability for negative fluxes. In the lhs. plots of Fig. 7 we show the ratios  $M_{+1}/M_0$  and  $M_{-1}/M_0$  as a function of  $\mu$  using  $\eta = 0.1$ . The Metropolis probabilities for accepting a step from  $k_{x,4} = 0$  to  $k_{x,4} = +1$  and  $k_{x,4} = -1$ , respectively are given by  $\max(1, M_{+1}/M_0)$  and  $\max(1, M_{-1}/M_0)$ . We see that for all  $\mu \neq 0$  we have  $M_{+1}/M_0 > M_{-1}/M_0$  and temporal fluxes  $k_{x,4} = +1$  are always favored over negative ones. For values of  $\mu$  up to  $\mu \sim 2.8$  the discrepancy between  $M_{+1}/M_0$  and  $M_{-1}/M_0$  remains large and the non-zero chemical potential pumps positive temporal  $k$ -flux into the system. However, this  $k$ -flux has to be compensated by plaquettes which costs Boltzmann weight and dampens the increase of temporal flux with  $k_{x,4} = +1$ . This interplay between the pumping with  $\mu$  and the damping by the Boltzmann factor of the plaquette variables can give rise to a phase transition at some critical value of  $\mu$ , when the positive temporal  $k$ -flux starts to dominate and drags along the plaquette occupation numbers. In the next subsection we will see that this is indeed the case for suitable values of the couplings.

It is, however, important to note that for  $\mu > 2.8$  the two ratios  $M_{+1}/M_0$  and  $M_{-1}/M_0$  start to approach each other again and they both have limit 1 for large  $\mu$ . This implies that at large values of  $\mu$  the probabilities for temporal fluxes  $k_{x,4} = +1$ ,  $k_{x,4} = 0$  and  $k_{x,4} = -1$  are equal, and the chemical potential does not favor an orientation for the  $k_{x,4}$ . Thus for sufficiently large  $\mu$  the Boltzmann factor of the plaquette occupation numbers may again dominate the physics. This raises an interesting question that then has to be answered in this region: How can the particle number density  $n$  keep growing with  $\mu$  if the weights  $M_s$  that drive the  $\mu$ -dependence for small  $\mu$  become degenerate at large  $\mu$ ? The answer lies in the flux representation of  $n$  given in (20): The numbers  $\mathcal{N}_s$ ,  $s \in \{+1, 0, -1\}$ , for temporal links with  $k_{x,4} = s$  are weighted with the factors  $R_s = M'_s/M_s$ . Also these ratios approach each other for large  $\mu$  and all three grow as  $e^\mu$  (rhs. plot in Fig. 7). Using  $\mathcal{N}_{+1} + \mathcal{N}_0 + \mathcal{N}_{-1} = N_s^3 N_t$  we conclude from (20) that for large  $\mu$  we have  $n \propto R_s \propto \eta e^\mu$ . In the plots for  $n$



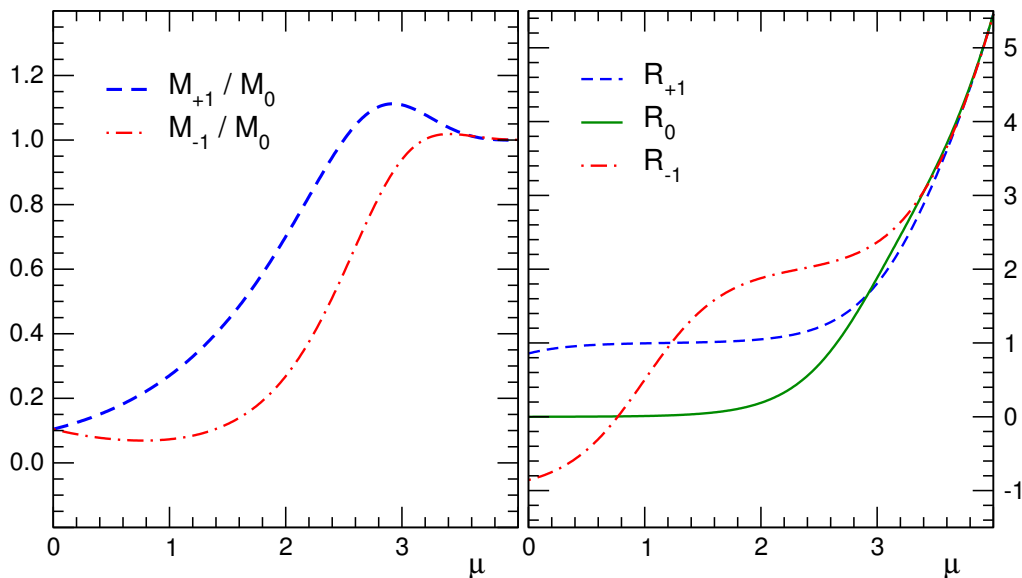


FIG. 7: Lhs.: The ratios  $M_{+1}/M_0$  and  $M_{-1}/M_0$  that determine the transition from temporal flux  $k_{x,4} = 0$  to  $k_{x,4} = +1$  and  $k_{x,4} = -1$  as a function of  $\mu$  at  $\eta = 0.1$ . Rhs.: The coefficients  $R_s = M'_s/M_s$  that determine the contributions of temporal flux  $k_{x,4} = s$  with  $s \in \{-1, 0, +1\}$  to the particle number density  $n$  in the dual representation (20).

and  $\chi_n$  of Fig. 8 we display these limiting curves and find that the Monte Carlo data nicely approach the expected asymptotic behavior. We found similarly good asymptotic behavior also for the weak coupling results shown in Fig. 11, but since there we use a smaller interval on the x-axis this is not entirely obvious from the plots.

It is a remarkable feature of the dual representation that part of the behavior of observables (e.g., the asymptotic behavior in the above example) is already encoded in the expansion factors of the partition sum and the representation of the observables in terms of dual variables.

### B. Finite density results at strong coupling

Let us now come to the numerical results at finite density. We numerically analyzed the finite density behavior for both values of  $\eta$  that were considered in Section IV, i.e.,  $\eta = 0.1$  and  $\eta = 0.5$ . For the  $\eta = 0.5$  case we did not find transitions as a function of  $\mu$  and thus do not present the corresponding results in this exploratory study. Instead we focus on  $\eta = 0.1$  and study the system for two couplings on both sides of the transition located at  $\beta_c \sim 0.7$ . We begin with the value  $\beta = 0.6$  in the strong coupling region in this subsection, continuing with  $\beta = 0.8$  in the weak coupling regime in the next subsection.

For the finite density study we use lattices of sizes  $N_s^3 \times 50$ , with  $N_s$  ranging from 2 to 12. The reason for the large  $N_t = 50$  is that we want to study the system at zero temperature. Although with  $N_t = 50$  the temperature  $T = 1/50 = 0.02$  in lattice units is not exactly zero, this value is much smaller than any other involved scale and constitutes a good approximation of  $T = 0$ . We consider

the full set of observables discussed in Section III, i.e., in addition to the plaquette  $\langle U \rangle$  and its susceptibility  $\chi_U$  we now also analyze the particle number density  $n$  and its susceptibility  $\chi_n$ .

In Fig. 8 we show the results for the four observables as a function of the chemical potential  $\mu$  and compare runs on  $N_s^3 \times 50$  lattices with different spatial extents  $N_s = 4, 8$  and  $12$ . The data for  $N_s = 8$  and  $N_s = 12$  fall on top of each other and only the  $N_s = 4$  data show a slight discrepancy near  $\mu \sim 2.57$  due to finite volume effects (the transition zone is shifted towards a slightly smaller  $\mu$ ). It is obvious that for  $\mu = \mu_c \sim 2.57$  the system undergoes a first order transition: Both first derivatives, the plaquette expectation value  $\langle U \rangle$  and the particle number density  $n$  show a clear discontinuity. The corresponding susceptibilities  $\chi_U$  and  $\chi_n$  diverge at  $\mu_c$ , which is, however, somewhat hard to see here since the transition is so sharp: As a matter of fact for very finely spaced values of  $\mu$  near  $\mu_c$  we find values for  $\chi_n$  that are three orders of magnitude larger than the scale used in the plot. A second indication that the transition is very narrow is the fact that only for  $N_s = 4$  we see small finite volume effects: The transition is shifted slightly to the left and appears somewhat rounded (at least for the first derivatives  $\langle U \rangle$  and  $n$ ). This trend towards visible finite size effects continues when using  $N_s = 2$  (data not shown).

Finally, a dataset at  $12^3 \times 100$ , which corresponds to an even lower temperature of  $T = 0.01$  in lattice units, falls on top of the  $12^3 \times 50$  data. We conclude that we reliably describe the situation at zero temperature, and that for  $\eta = 0.1$  and  $\beta = 0.6$  the system undergoes a very narrow first order transition at  $\mu_c \sim 2.57$ .

From the fact that the plaquette undergoes such a dras-

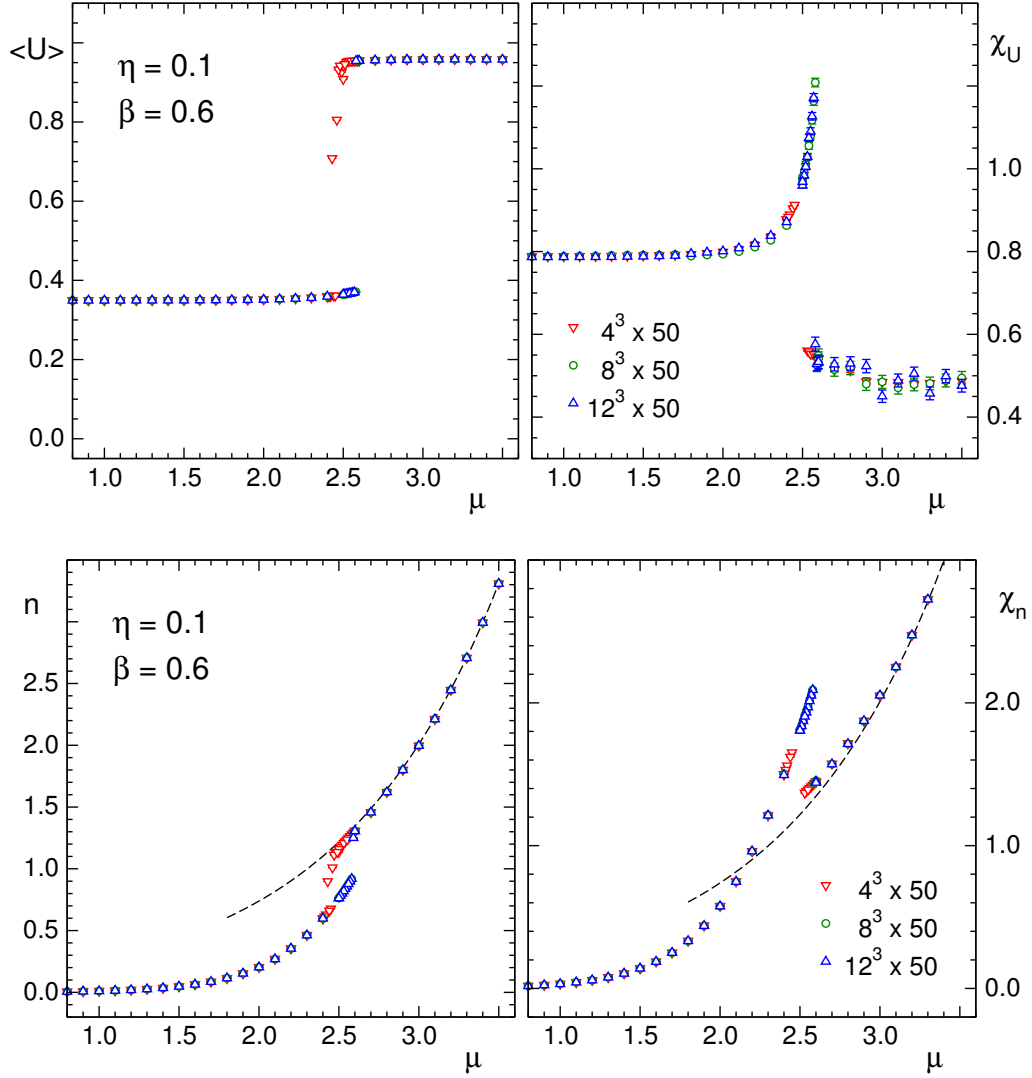


FIG. 8: Results for  $\langle U \rangle$ ,  $\chi_U$ ,  $n$  and  $\chi_n$  in the strong coupling region of  $Z_3$  Gauge-Higgs theory ( $\eta = 0.1$  and  $\beta = 0.6$ ) as a function of the chemical potential  $\mu$ . We compare the results for three different spatial volumes with  $N_s = 4, 8$  and  $12$ . The dashed curves in the plots for  $n$  and  $\chi_n$  are the asymptotic curves expected from the behavior of the coefficients  $M_s$  for large  $\mu$  (see the discussion in Subsection V-A.).

tic change at  $\mu_c$  we conclude that the gauge dynamics plays an important role in the transition. This is also reflected in the finding that the critical value  $\mu_c$  depends on  $\beta$ . For  $\beta = 0.6$  we observed  $\mu_c \sim 2.57$ , while for  $\beta = 0.65$  it is at  $\mu_c \sim 2.35$ , and  $\mu_c \sim 3.0$  for  $\beta = 0.55$ .

Finally we point out that for large  $\mu$  the results for  $n$  and  $\chi_n$  approach the asymptotic curves  $\propto \eta \exp(\mu)$  (dashed lines in the plots) which we derived in Subsection V-A. from the behavior of the coefficients  $M_s$ .

To further understand the nature of the transition, in Fig. 9 we show 3-D illustrations of the plaquette and flux occupation numbers for a value of  $\mu = 2.4 < \mu_c$  (top row of plots) and  $\mu = 2.7 > \mu_c$ . We consider 3-dimensional sections of the 4-dimensional lattice with only spatial directions (lhs. pair of plots in each row) and 3-dimensional sections with the vertical direction being time (rhs. pair

of plots). In each pair the lhs. section illustrates the plaquette occupation numbers (plaquettes with  $p = +1$  are blue, those with  $p = -1$  are red), while the rhs. section of each pair displays the corresponding fluxes (links with  $k = +1$  are blue, those with  $k = -1$  are red).

It is obvious that below  $\mu_c$  (top row of plots) the occupation numbers for plaquettes and for fluxes are very small, while for  $\mu > \mu_c$  (bottom) we see a large abundance of non-zero occupation numbers. The transition thus is between a dilute phase where all occupation numbers are small and a condensed phase characterized by high occupation numbers for both, fluxes and plaquettes. Furthermore, a close inspection of the 3-D plot for the fluxes at  $\mu > \mu_c$  on the temporal section (lower right plot) shows that positive temporal flux (vertical blue lines in the plot) dominates, as expected from the finite density

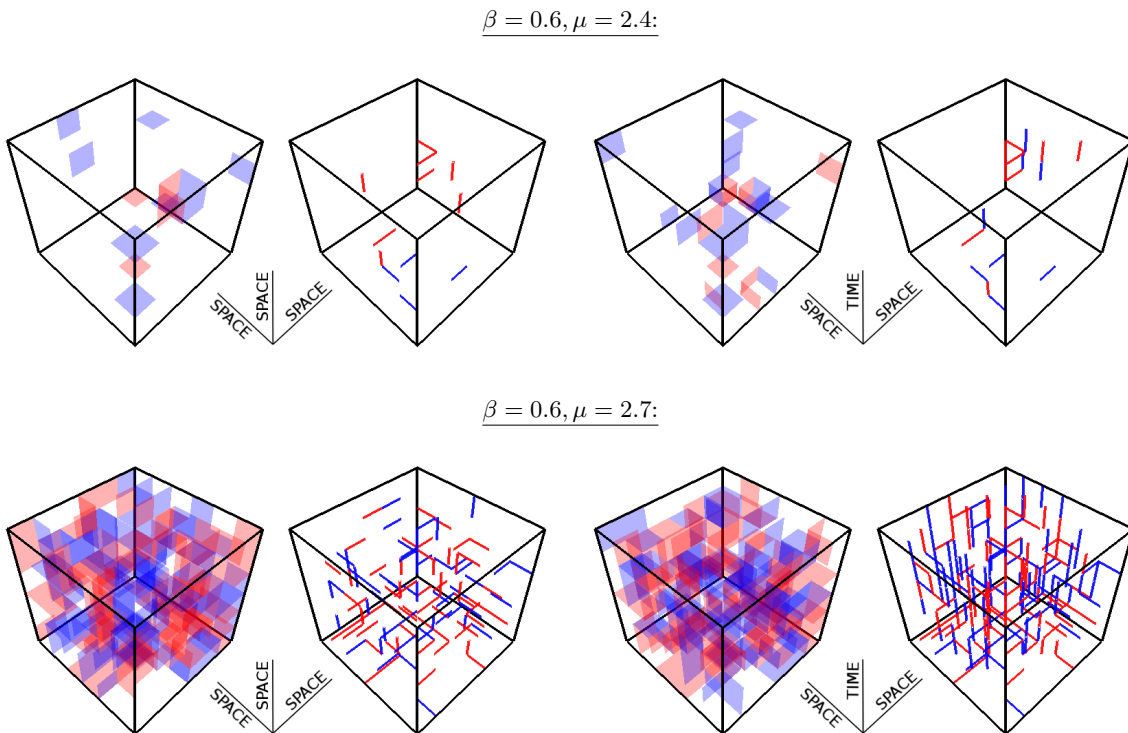


FIG. 9: 3-D illustration of typical configurations of plaquette occupation numbers  $p$  and fluxes  $k$  in the strong coupling phase ( $\beta = 0.6, \eta = 0.1$ ) for  $\mu = 2.4 < \mu_c$  (top row of plots) and for  $\mu = 2.7 > \mu_c$  (bottom). We use 3-dimensional sections of the lattice embedded in 4 dimensions and show purely spatial sections (1st and 2nd plot in each row) and sections where the vertical direction is time (3rd and 4th plot). In each pair the lhs. section shows the non-trivial plaquette occupation numbers and we use blue for plaquettes with  $p = +1$  and red for  $p = -1$ . Likewise, in the rhs. plot of each pair we show the non-trivial link variables with blue links for  $k = 1$  and red for  $k = -1$ .

picture in terms of the dual variables discussed in the previous subsection.

We remark at this point that the value of  $\langle U \rangle \sim 0.35$  which we observe below  $\mu_c$  is mainly due to the constant term in the dual representation (18). Here we use  $\beta = 0.6$  for the inverse gauge coupling and the constant term has a value of 0.327. Thus also at very low plaquette occupation numbers  $p$  the plaquette has a value of  $\langle U \rangle \sim 0.35$  at  $\beta = 0.6$ . The jump of  $\langle U \rangle \sim$  from 0.35 to almost 1 at  $\mu_c$  is due to the condensation of non-trivial plaquette occupation numbers  $p$  as is obvious from Fig. 9.

To further illuminate the picture of a condensation of the plaquette occupation numbers triggered by temporal  $k$ -flux enhanced by  $\mu$ , we now look at plots for the occupation numbers for plaquettes and fluxes as a function of the chemical potential  $\mu$ . Fig. 10 shows the number of non-trivial spatial plaquettes  $P_s$ , i.e., the total number of  $p_{x,\sigma\tau} \neq 0$ , the number of temporal non-trivial plaquettes  $P_t$  ( $p_{x,\sigma 4} \neq 0$ ), the number of non-trivial spatial fluxes  $S$  ( $k_{x,j} \neq 0$ ), and the numbers of positive and negative temporal fluxes  $T_+$  and  $T_-$  ( $k_{x,4} = +1$  and  $k_{x,4} = -1$ ). All these occupation numbers are normalized such that the maximally possible occupation number is 1.

The occupation numbers for spatial ( $P_s$ ) and temporal ( $P_t$ ) plaquettes essentially vanish below  $\mu_c$  and then take

a jump where both show an occupation of roughly 0.37, with the temporal plaquettes slightly enhanced. This behavior clearly reflects the condensation of the plaquettes we had discussed above. Similarly the occupation number  $S$  for the spatial flux nearly vanishes below  $\mu_c$  where it jumps to a finite value. The occupation numbers for positive and negative temporal flux,  $T_+$  and  $T_-$  show an interesting behavior: Both essentially vanish below  $\mu_c$ . At the transition their degeneracy is lifted and both jump to different values. As the chemical potential is increased further the occupation numbers for positive and negative temporal flux both approach the value  $1/3$  (marked by a dashed horizontal line) which is the value one expects when the corresponding Boltzmann weights  $M_s$  become degenerate (see the discussion in the previous subsection where we analyzed the behavior of the weight factors  $M_s$  shown in Fig. 7).

### C. Finite density results at weak coupling

We continue with the discussion of the finite density behavior for the weak coupling region, i.e., for  $\beta = 0.8$  and again  $\eta = 0.1$ . Here the situation is different since in the weak coupling phase already at  $\mu = 0$  we have

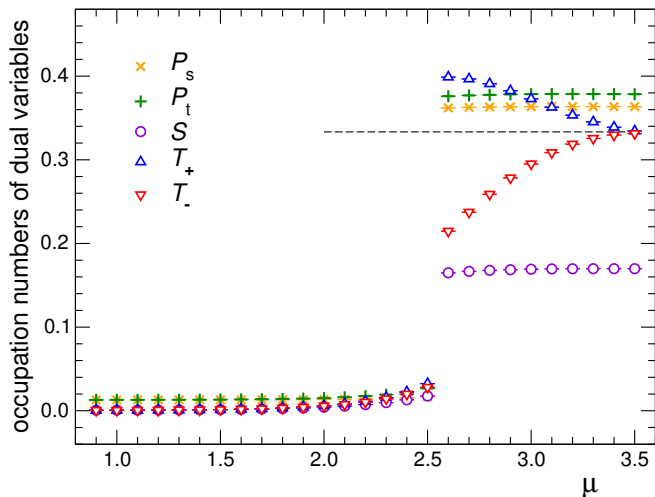


FIG. 10: Occupation numbers for the dual variables at strong coupling ( $\beta = 0.6, \eta = 0.1$ ) as a function of  $\mu$  from our  $12^4 \times 50$  lattices. We show the number of non-trivial spatial plaquettes  $P_s$ , i.e., the total number of  $p_{x,\sigma\tau} \neq 0$ , the number of temporal non-trivial plaquettes  $P_t$  ( $p_{x,\sigma 4} \neq 0$ ), the number of non-trivial spatial fluxes  $S$  ( $k_{x,j} \neq 0$ ), and the numbers of positive and negative temporal fluxes  $T_+$  and  $T_-$  ( $k_{x,4} = +1$  and  $k_{x,4} = -1$ , respectively). All occupation numbers are given as intensive quantities, normalized such that the maximally possible occupation number is 1. The horizontal line marks the value  $1/3$  which the occupation numbers  $T_+$  and  $T_-$  are expected to approach for large  $\mu$ .

$\langle U \rangle \sim 1$ , i.e., the plaquette occupation numbers are already condensed. As in the previous subsection we consider the plaquette  $\langle U \rangle$ , its susceptibility  $\chi_U$ , the particle number density  $n$  and the corresponding susceptibility  $\chi_n$ . In Fig. 11 we show our results as a function of  $\mu$ , comparing runs on  $N_s^3 \times 50$  lattices with different spatial extents  $N_s = 4, 8$  and  $12$ .

The susceptibility  $\chi_n$  shows clearly that also in the weak coupling regime at  $\beta = 0.8$  we find a phase transition which is located at  $\mu_c \sim 1.35$ . Inspection of the particle number density shows that  $n$  has a discontinuity at  $\mu_c$  and we are again dealing with a first order transition here. As for the transition in the strong coupling regime which we discussed in the last subsection, also here the finite volume effects are rather small and are visible only for the  $N_s = 4$  data. The transition is very narrow and as before we remark that the maxima in our data for  $\chi_n$  are much higher than the range used for the vertical axis.

For the plaquette expectation value  $\langle U \rangle$  the situation is different from the strong coupling phase of the last subsection. Since here we start with  $\langle U \rangle \sim 1$  below  $\mu_c$ , the change of  $\langle U \rangle$  at  $\mu_c$  is rather unspectacular with the plaquette simply developing a mild slope. Correspondingly the susceptibility  $\chi_U$  shows a slight drop above  $\mu_c$  as the plaquette numbers become completely saturated. We conclude that the transition in the weak coupling phase is predominantly driven by the matter fields, i.e.,

the flux variables  $k$  in the dual language. This finding is supported by the fact that changing the coupling  $\beta$  from 0.8 to nearby values in the weak coupling regime ( $\beta = 0.75$  and  $\beta = 0.85$ ) has no noticeable effect on the value of  $\mu_c$ . This underlines the statement that the transition is driven by the flux variables in the background of condensed plaquette occupation numbers  $p$ .

Again we also compare the results for  $n$  and  $\chi_n$  to the expected asymptotic behavior (dashed curves in the plot). We found that as in the strong coupling case the lattice data very nicely approach the expected asymptotic behavior (although this is not very clearly visible for the range of  $\mu$ -values chosen in Fig. 11).

In order to analyze the nature of the transition in the weak coupling regime, in Fig. 12 we repeat the 3-D illustration of the plaquette occupation numbers and fluxes of the previous subsection. It is obvious that the plaquette occupation numbers are large on both sides of the transition, and the fluxes undergo their transition in a condensed medium of plaquette occupation numbers. The flux transition is again manifest in an abrupt increase of flux, although with a smaller amplitude than in the strong coupling phase. As before we see a dominance of positive temporal flux above  $\mu_c$ , i.e., vertical blue lines in the lower right plot.

We conclude the discussion of the transition in terms of the dual variables by again analyzing the occupation numbers as a function of the chemical potential. In Fig. 13 we show the weak coupling results for non-trivial occupation numbers of spatial and temporal plaquettes ( $P_s, P_t$ ), of spatial flux ( $S$ ), and the occupation numbers for positive and negative temporal flux ( $T_+, T_-$ ). We use the same definitions as in Fig. 10 for the strong coupling phase. Obviously the plaquette occupation numbers are large for all values of  $\mu$ , and only a very mild change at  $\mu_c \sim 1.35$  is visible. The flux variables show a small step at  $\mu_c$  which, however, is less pronounced than in the strong coupling case. Again we observe a strong splitting between the positive and negative temporal fluxes which reflects the influence of the chemical potential. At the largest values of  $\mu$  we observe that the occupation numbers for positive and negative temporal flux approach each other in agreement with the physical picture developed on the discussion of Fig. 7.

## VI. SUMMARY AND DISCUSSION

In this article we explored the possibility of a dual simulation of gauge theories with matter fields. Although our study is for a simple model, the  $Z_3$  Gauge-Higgs model, it captures some of the features that are expected also for more interesting theories, in particular the appearance of surfaces for the gauge fields and loops of flux for matter. In addition it was demonstrated that the complex action problem of the conventional representation at non-zero chemical potential is solved in the dual approach.

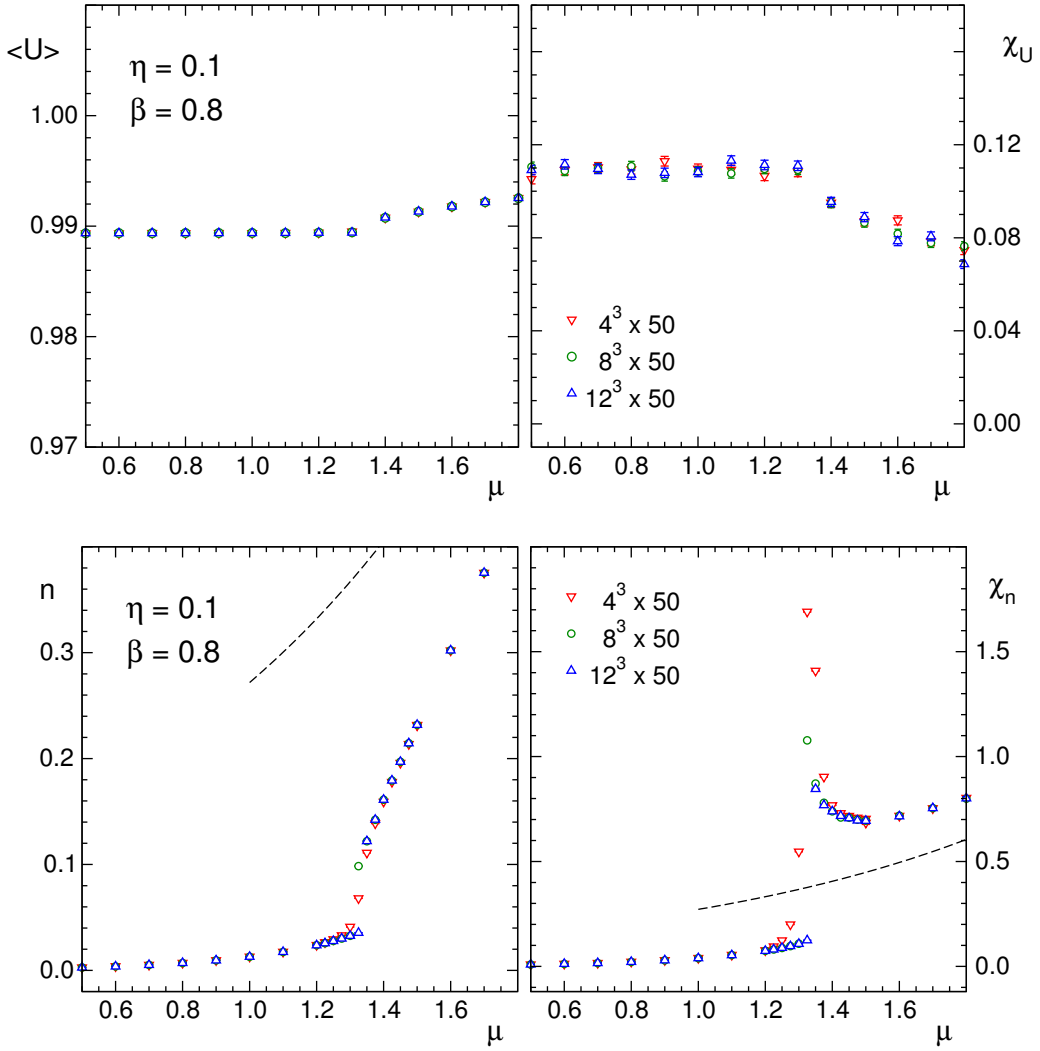


FIG. 11: Results for  $\langle U \rangle$ ,  $\chi_U$ ,  $n$  and  $\chi_n$  in the weak coupling regime of  $Z_3$  Gauge-Higgs theory ( $\eta = 0.1$  and  $\beta = 0.8$ ) as a function of the chemical potential  $\mu$ . We compare the results for three different spatial volumes with  $N_s = 4, 8$  and  $12$ . The dashed curves in the bottom plots represent the asymptotic behavior of  $n$  and  $\chi_n$  at large  $\mu$ .

A suitable Monte Carlo update was developed which properly treats the constraints of flux conservation at the sites and the surface constraints based at the links of the lattice (both constraints are modulo 3). In a detailed comparison in the pure gauge case and at vanishing chemical potential it was shown that the dual approach and the algorithm reproduce the results from a simulation in the conventional representation, thus establishing the validity of the dual approach.

To test the approach at finite chemical potential  $\mu$  where conventional techniques fail, we explored the behavior of observables as a function of  $\mu$  for two sets of couplings in the strong and weak coupling domains. In both cases we found first order transitions which were discussed not only based on usual observables, but also in terms of occupation numbers for the dual variables. We stress at this point that our two case studies in the strong and weak coupling regimes do of course not con-

stitute a systematic analysis of the phase diagram for the  $Z_3$  Gauge-Higgs model – a task we do not aim at here.

The techniques developed in this paper can easily be generalized to other Gauge-Higgs systems with abelian groups [18]. The dual degrees of freedom are again surfaces and loops of flux, although the structure of the constraints and the weight factors will differ for other abelian groups. Some of the aspects and properties found in the  $Z_3$  system might, however, turn out to be universal features of a dual approach:

- The dual formulation represents the system using only gauge invariant degrees of freedom, i.e., suitable occupation numbers for the plaquettes and the gauge invariant nearest neighbor terms of the matter fields.
- Part of the dynamics is encoded in expansion coefficients of the partition sum and the observables

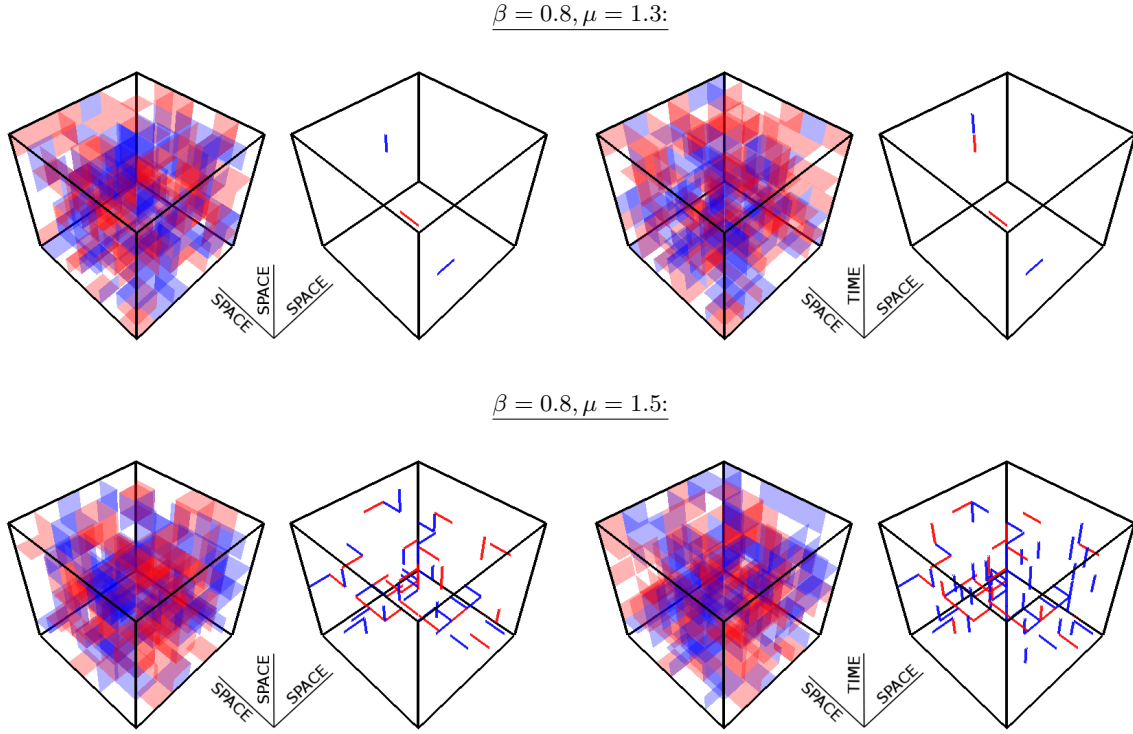


FIG. 12: 3-D illustration of typical configurations of plaquette occupation numbers  $p$  and fluxes  $k$  in the weak coupling phase ( $\beta = 0.8, \eta = 0.1$ ) for  $\mu = 1.3 < \mu_c$  (top row of plots) and for  $\mu = 1.5 > \mu_c$  (bottom). We use 3-dimensional sections through the lattice embedded in 4 dimensions and show purely spatial sections (1st and 2nd plot in each row) and sections where the vertical direction is time (3rd and 4th plot). In each pair the lhs. plot shows the non-trivial plaquette occupation numbers and we use blue for plaquettes with  $p = +1$  and red for  $p = -1$ . Likewise, in the rhs. plot of each pair we show the non-trivial link variables with blue links for  $k = 1$  and red for  $k = -1$ .

(e.g., the asymptotic  $\mu$ -behavior in the system studied here).

- Suitable Monte Carlo algorithms turn out to be rather simple, and at least for some cases a worm-type generalization to surfaces may be possible.
- The dual representation is not only a tool to solve the complex action problem, but also allows for a conclusive discussion of the mechanisms at the various phase transitions in terms of the dual variables.

It is obvious that the current results only present first steps towards the more important cases of non-abelian gauge fields or systems with fermions. Nevertheless we expect that some of the techniques developed in the dual approach to abelian Gauge-Higgs systems might prove useful also for these more interesting cases.

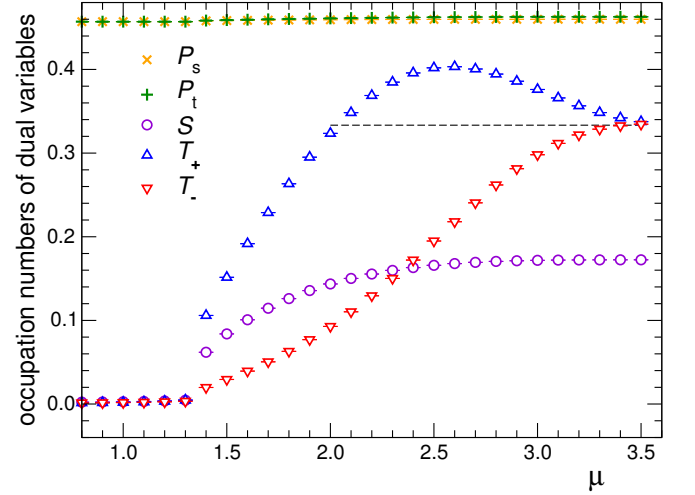


FIG. 13: Same as Fig. 11 now at  $\beta = 0.8, \eta = 0.1$ : We show the number of non-trivial spatial plaquettes  $P_s$ , the number of temporal non-trivial plaquettes  $P_t$ , the number of non-trivial spatial fluxes  $S$  and the numbers of positive and negative temporal fluxes  $T_+$  and  $T_-$ . The horizontal line marks the asymptotic value  $1/3$  for  $T_+$  and  $T_-$ .

**Acknowledgements:** The authors would like to thank Shailesh Chandrasekharan, Ydalia Delgado Mercado, Philippe de Forcrand, David Kaplan, Thomas Kloiber, Christian Lang and Anyi Li for interesting discussions and remarks on the literature. A.S. is funded by the FWF DK W1203 "Hadrons in Vacuum, Nuclei and Stars". C.G. acknowledges support from the Dr. Heinrich Jörg

foundation of the Karl-Franzens-University, Graz. C.G. also thanks the members of the INT at the University of Washington, Seattle where part of this work was done for hospitality and support. This work is also partly supported by DFG TR55, *Hadron Properties from Lattice QCD*.

- 
- [1] S. Gupta, PoS LATTICE **2010**, 007 (2010) [arXiv:1101.0109]. P. de Forcrand, PoS LAT **2009**, 010 (2009) [arXiv:1005.0539].
- [2] S. Chandrasekharan, PoS LATTICE **2008** (2008) 003 [arXiv:0810.2419].
- [3] N. Prokof'ev and B. Svistunov, Phys. Rev. Lett. **87** (2001) 160601.
- [4] C. Gattringer, V. Hermann and M. Limmer, Phys. Rev. D **76** (2007) 014503, [arXiv:0704.2277]. U. Wolff, Nucl. Phys. B **789** (2008) 258, [arXiv:0707.2872]. U. Wenger, Phys. Rev. D **80**, 071503 (2009), [arXiv:0812.3565]. Nucl. Phys. B **814**, 549 (2009), [arXiv:0812.0677]. O. Bär, W. Rath and U. Wolff, Nucl. Phys. B **822**, 408 (2009), [arXiv:0905.4417]. M. G. Endres, Phys. Rev. A **85**, 063624 (2012), [arXiv:1204.6182 [hep-lat]].
- [5] F. Karsch and K. H. Mütter, Nucl. Phys. B **313** (1989) 541. S. Chandrasekharan and F.J. Jiang, Phys. Rev. D **68** (2003) 091501, [arXiv:hep-lat/0309025]. D.H. Adams and S. Chandrasekharan, Nucl. Phys. B **662** (2003) 220, [arXiv:hep-lat/0303003]. P. de Forcrand and M. Fromm, Phys. Rev. Lett. **104** (2010) 112005 [arXiv:0907.1915]. P. de Forcrand, M. Fromm, J. Langelage, K. Miura, O. Philipsen and W. Unger, arXiv:1111.4677. S. Chandrasekharan and A. Li, JHEP **1101** (2011) 018 [arXiv:1008.5146].
- [6] S. Chandrasekharan and A. Li, Phys. Rev. D **85**, 091502 (2012) [arXiv:1202.6572 [hep-lat]]; Phys. Rev. Lett. **108**, 140404 (2012) [arXiv:1111.7204 [hep-lat]]; PoS LATTICE **2011** (2011) 058 [arXiv:1111.5276 [hep-lat]].
- [7] Y.D. Mercado, H.G. Evertz and C. Gattringer, Phys. Rev. Lett. **106** (2011) 222001, [arXiv:1102.3096]; Acta Phys. Polon. Supp. **4** (2011) 703, [arXiv:1110.6862]; Comput. Phys. Commun. **183** (2012) 1920 [arXiv:1202.4293 [hep-lat]]. C. Gattringer, Nucl. Phys. B **850** (2011) 242, [arXiv:1104.2503]. Y. Delgado, H. G. Evertz, C. Gattringer and D. Göschl, PoS Lattice2011, [arXiv:1111.0916].
- [8] M. Fromm, J. Langelage, S. Lottini and O. Philipsen, JHEP **1201**, 042 (2012) [arXiv:1111.4953 [hep-lat]]; arXiv:1207.3005 [hep-lat].
- [9] M. Hogervorst and U. Wolff, Nucl. Phys. B **855**, 885 (2012), [arXiv:1109.6186]. T. Korzec, I. Vierhaus and U. Wolff, Comput. Phys. Commun. **182**, 1477 (2011), [arXiv:1101.3452]. P. Weisz and U. Wolff, Nucl. Phys. B **846** 316 (2011), [arXiv:1012.0404]. U. Wolff, Nucl. Phys. B **832**, 520 (2010), [arXiv:1001.2231]; Nucl. Phys. B **824**, 254 (2010) [Erratum-ibid. **834**, 395 (2010)], [arXiv:0908.0284].
- [10] M. G. Endres, Phys. Rev. D **75**, 065012 (2007), [hep-lat/0610029]; PoS LAT **2006**, 133 (2006), [hep-lat/0609037].
- [11] T. Sterling and J. Greensite, Nucl. Phys. B **220**, 327 (1983). M. Panero, JHEP **0505**, 066 (2005), [hep-lat/0503024]. V. Azcoiti, E. Follana, A. Vaquero and G. Di Carlo, JHEP **0908**, 008 (2009), [arXiv:0905.0639].
- [12] T. Korzec and U. Wolff, PoS LATTICE **2010** (2010) 029 [arXiv:1011.1359].
- [13] S. Chandrasekharan and U. -J. Wiese, Phys. Rev. Lett. **83**, 3116 (1999) [cond-mat/9902128].
- [14] G. Aarts, Phys. Rev. Lett. **102** (2009) 131601 [arXiv:0810.2089].
- [15] G. Aarts, JHEP **0905** (2009) 052, [arXiv:0902.4686].
- [16] C. Gattringer and T. Kloiber, arXiv:1206.2954 [hep-lat].
- [17] Y. Delgado-Mercado, A. Schmidt, in preparation.
- [18] C. Gattringer, A. Schmidt, in preparation.
- [19] B. Lautrup and M. Nauenberg, Phys. Lett. **95 B**, 63 (1980). R. Horsley and U. Wolff, Phys. Lett. **105 B**, 290 (1981).
- [20] It is straightforward to derive the dual representation for several correlators and also for Wilson loops by introducing locally varying couplings, taking suitable derivatives and then setting the couplings back to the values one wants to work at. In our exploratory analysis of the  $Z_3$  Gauge-Higgs systems with dual variables we do not present results for this type of observables.
- [21] Also for gauge group  $U(1)$  the dual representation of pure gauge theory consists of closed surfaces, but the plaquette occupation numbers assume values in the integers  $\mathbb{Z}$ .